Materials Transactions, JIM, Vol. 36, No. 2 (1995), pp. 357 to 364

Mössbauer Effect Studies of Fe-Base Alloys during Mechanical Alloying and Grinding (*Overview*)

A. F. Cabrera, M. B. Fernández van Raap, M. Meyer, C. Rodríguez Torres, L. Mendoza-Zélis and F. H. Sánchez

Departamento de Física, Facultad de Ciencias Exactas, Universidad Nacional de La Plata, C. C. 67, 1900 La Plata, República Argentina

Mössbauer effect studies of mechanical alloying and mechanical grinding of Fe-B, Fe-Sn and Fe-TM-Al (TM=Ni, Cu), complemented by X-ray diffraction analysis are presented. Some of these systems (Fe-Sn) are especially suited for these type of research because the environments of both elements can be probed. In all cases powders were processed with a Retsch MM 2 horizontal vibratory mill under argon atmosphere.

In $Fe_{1-x}Sn_x$ ($0.15 \leq x \leq 0.40$), the evolution of mechanical alloying with time and the dependence of the stationary state with composition were investigated. An intermediate superparamagnetic $FeSn_2$ state and a stationary bcc solid solution with composition fluctuations were inferred from the Mössbauer spectra. Solubility of tin into bcc iron was found to be extended up to a maximum of about 22 at.%.

Pure powder mixtures of nominal composition $Al_{75}Ni_{10}Fe_{15}$, $Al_{65}Ni_{20}Fe_{15}$ and $Al_{63}Cu_{25}Fe_{12}$ have been mechanically alloyed. Stable disordered crystalline phases were obtained after milling and, in some cases, the partial ordering of bcc structures induced by milling was observed. Further annealings did not produce structural changes but removed the remaining disorder. The characteristic quadrupole interaction parameters were obtained by Mössbauer spectroscopy.

The evolution of Fe_2B with grinding time was studied. The first milling stage was characterized by fragmentation and accumulation of strain. On further processing, segregation of α-Fe occurred while grain size reduction continued and strain was partially removed. For longer grinding times separation of α-Fe proceeded at an almost steady rate. Two additional experiments designed to reduce and increase oxygen contamination let us tentatively discard this element as the main responsible for the observed decomposition.

(Received October 25, 1994)

Keywords: *Mössbauer effect, iron-tin, aluminum-nickel-iron, aluminum-copper-iron, iron-boron, solid solutions, local atomic environments.*

I. Introduction

Hyperfine Interaction techniques, such as Mössbauer effect (ME) and perturbed angular correlation (PAC) spectroscopy, may prove useful in mechanical alloying (MA) and mechanical grinding (MG) research. The distinguishing feature of these nuclear methods is their ability of sensing the surroundings of a given isotope used as a probe. The combination of the information obtained by ME and PAC with that coming from X-ray diffraction (XRD) should help to understand whether the observed signals originate in short range or in long range ordered structures. This potential resolution is desirable in MA and MG investigations since it would provide the possibility of detecting and identifying nanoscopically dispersed phases and local atomic arrangements. Some of the ME and PAC most oustanding features for MA and MG research are the following:

- The observation of local magnetic properties, such as the hyperfine field (H) at the nuclear site.
- The determination of electronic properties, such as the charge density (isomer shift δ) and the electric field gradient (EFG) at the nuclear site. Normally, the measurement of two of these three quantities is enough to identify a particular phase.
- The fact that in many situations both H and δ vary almost linearly with the number of near neighbours of a given class. This feature allows the analysis of solid solutions, including compound stoichiometry deviations.
- The strong dependence of the EFG with the symmetry of the charge distribution. This information may help to detect local deviations from equilibrium structures.
- The sensitivity to dynamic processes. One example of these is superparamagnetism, i.e. the collapse of the magnetic hyperfine interaction when thermal energy kT becomes of the order of the magnetic anisotropic energy KV (K being the magnetic anisotropic energy density and V the volume of single domain grains). As the collapse occurs typically for crystallites of less than about 10 nm, this phenomenon is helpful in the determination of the approximate grain size.

On the other hand, the use of these nuclear methods restricts MA and MG research to systems containing appropriate ME and PAC probes, among which are ^{181}Hf, ^{111}In (PAC), and ^{57}Fe and ^{119}Sn (ME). In this paper we review our recent investigations in the Fe-m (m=B, Sn) and Al-Fe-TM (TM=Ni, Cu) systems. These studies are focussed on different subjects: MG induced transformations in the case of Fe_2B; formation of extended range solid solutions by MA in the case of Fe-Sn; and production of quasicrystals and related phases by MA for Al-

Fe-TM systems.

It is worth mentioning that other hyperfine studies on the MG and MA in the systems Hf-Fe, Fe-Si, Fe-Ge and Fe-Ni-B and the mechanically induced disorder in spinel structures are currently in progress.

II. Experimental

All samples were preapared using high purity elements in powder form. For MA, typical starting particle size ranged from about 2 to 40 μm, but larger initial particle size was allowed for some of the MG experiments. Elemental powders premixed with appropriate nominal compositions (MA) or compound powders (MG) were sealed in chrome steel cylindric vials (5 cm^3) under Ar (0.9998) atmosphere along with one stainless steel milling ball (9 mm diameter). In most experiments a ball to powder mass ratio of about 10 was used. Milling was performed with a Retsch MM 2 horizontal vibratory mixer mill operated at a frequency of about 30 Hz.

ME experiments were carried out with conventional spectrometers under transmission geometry, employing ^{57}CoRh and Ca^{119}SnO$_3$ radioactive sources. All quoted isomer shifts are relative to α-Fe or $CaSnO_3$ respectively. XRD patterns were obtained in reflection geometry using a Philips PW1710 diffractometer with Cu $K\alpha$ radiation. All measurements were performed at room temperature.

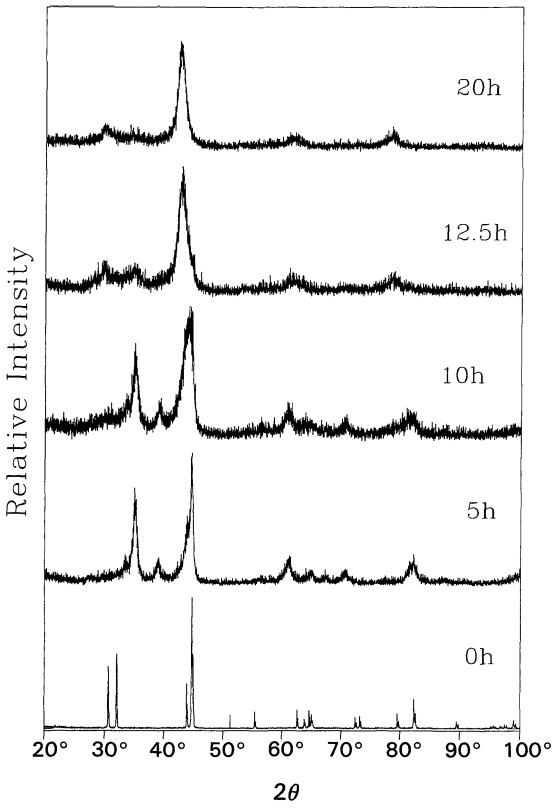

Fig. 1 XRD patterns of mechanically alloyed $Fe_{0.70}Sn_{0.30}$ as a function of milling time t.

III. Results

1. Mechanical alloying of $Fe_{1-x}Sn_x$ ($0.15 \leq x \leq 0.40$)

MA of $Fe_{1-x}Sn_x$ has been previously performed for two compositions ($x=0.67$[1] and $x=0.25$[2]). In the second case the formation of single phase bcc solid solution was reported. The occurrence of a large solubility of tin into iron is not expected for two reasons. First, the enthalpy of mixing is slightly positive (0–12 kJ/mol)[3]. Second, a large elastic contribution is expected since Fe and Sn atomic radii differ by about 30 percent. Our research on this system was mainly addressed to the observation of short range order evolution with milling time, to the determination of solubility limits for Sn in Fe under our MA conditions, and to the study of the homogeneity of the bcc solid solution. This project is part of a systematic MA and MG study on the Fe-m systems (m=Sn, Ge, Si).

Figure 1 shows diffractograms of $Fe_{0.70}Sn_{0.30}$ after several milling times t. They indicate the formation and growth of $FeSn_2$ until all tin is exhausted ($t \leq 5$ h). During this stage the material becomes sticky, eventually producing the adhesion of the ball to the vial wall. For longer times the formation of a bcc Fe(Sn) solid solution follows. In the final stationary state ($t \geq 15$ h) all reflections, with the exception of one located at $2\theta \approx 30°$, correspond to this phase. According to the bcc lattice parameter ($a \approx 0.3$ nm) a maximum Sn atomic concentration of about 22% is attained which is considerably beyond the solubility of tin into iron. The evolution of mean grain size with t obtained from the analysis of the diffractograms, is shown in Fig. 2.

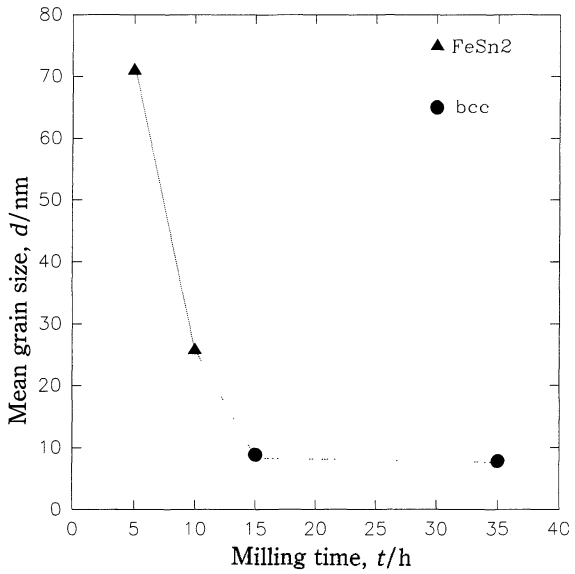

Fig. 2 Mean size of $FeSn_2$ and bcc solid solution grains as a function of milling time t.

The ME spectra of the same samples confirm these results[4]. The ME signal indicates that $FeSn_2$ crystallites of less or equal than about 70 nm are in superparamagnetic state. From the behaviour of the ^{57}Fe and ^{119}Sn H- and δ-distributions, the existence of composition fluctuations in the final bcc solid solution can be inferred, which

will be discussed below. In addition, another (minority) distribution was needed in order to describe properly the ^{57}Fe spectra of the stationary state, corresponding to tin rich environments of nearly uniform local coordination (sharp peak at $\delta \approx 0.52$–0.55 mm/s). These environments may be responsible for the XRD reflection at 30°.

The diffractograms corresponding to the stationary states ($0.15 \leq x \leq 0.30$) or long milling times (40 h, $x=0.40$) are similar to that at the top of Fig. 1, but with no reflections in the range $2\theta < 43°$ for $x=0.15$, 0.20. Figures 3 and 4 show the ME results of these samples. The spectra indicate that when x decreases the ME signals

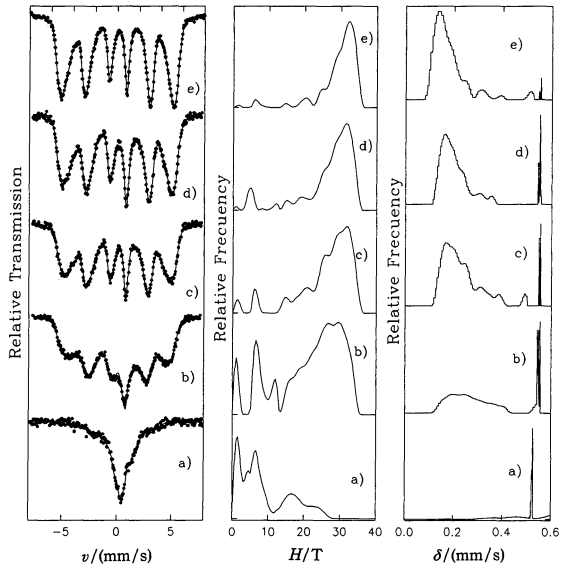

Fig. 3 ^{57}Fe ME results for $Fe_{1-x}Sn_x$ long MA runs as a function of composition. From left to right: ME spectra, H-distributions, and δ-distributions. Plots a) to e) correspond to $x=0.40$, 0.30, 0.25, 0.20 and 0.15. For $x \leq 0.30$ the results correspond to the stationary states.

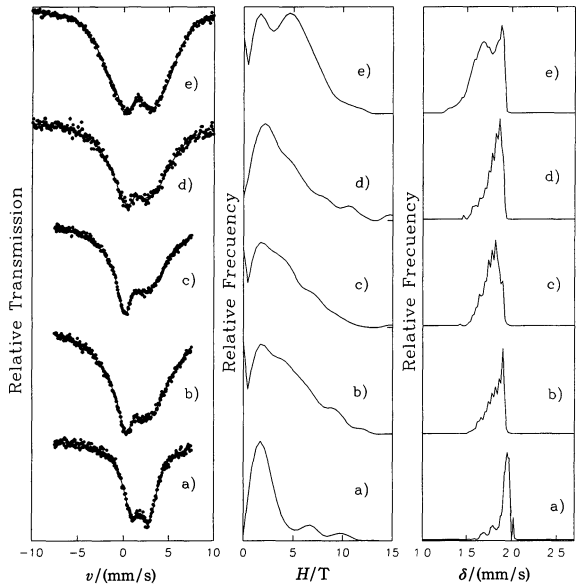

Fig. 4 Same as Fig. 3 but for ^{119}Sn.

become better defined and mean hyperfine fields increase. The part of the total H-distributions spreading to high fields is associated with the bcc solution. It corresponds to the body of the δ-distributions which spread towards the left. The distributions behaviour is reasonable since, for both ^{57}Fe and ^{119}Sn, H reduces and δ increases with the number of Sn near neighbours (nn). The width of the part of the isomer shift distribution assigned to the bcc phase is consistent with the rate of growth of δ with the number N of Sn nn observed in less concentrated alloys ($d\delta(^{57}Fe)/dN \approx 0.04$ mm/s)[5][6]. However, for $x \leq 0.30$, ^{57}Fe and ^{119}Sn distributions are peaked at high iron and high tin coordination numbers respectively indicating important composition fluctuations. These fluctuations suggest that in the solid solution iron and tin tend to remain as much separated as possible, as it should be expected on the basis of energy considerations. Histograms for Sn and Fe nn can be derived from these distributions[4]. It can be noted that the relative area of the narrow contribution to the ^{57}Fe δ-distribution located at about 0.53 mm/s decreases with x and almost vanishes for $x=0.15$. For $x=0.40$ the ^{57}Fe distributions are no longer peaked at high iron nn numbers. This is probably because of the larger Sn concentration but it also reflects the formation and growing importance of other phases. In fact X-ray diffractograms taken from this sample basically correspond to a mixture of the solid solution and disordered FeSn.

In summary, the combination of XRD and ^{57}Fe and ^{119}Sn ME studies to the study of the MA of Fe and Sn powders allows the following conclusions:

i) Mixing begins with coating of the iron particles with tin. In this state the material becomes highly sticky. ($t \approx 0$–3 h).

ii) The solid state reaction (SSR) $Fe + Sn \rightarrow FeSn_2$ proceeds at the Fe/Sn interface until all Sn is exhausted. The system losses its sticky properties. Formed $FeSn_2$ is superparamagnetic. This state occurs for crystallite size of less or equal than about 70 nm. ($t \approx 0$–5 h).

iii) The SSR α-$Fe + FeSn_2 \rightarrow \alpha$-Fe(Sn) occurs by diffusion of tin into iron. A metastable bcc solid solution forms with tin concentration of up to about 22 at.%, i.e., far beyond the solubility limit. The bcc lattice parameter becomes of the order of 0.3 nm. ($t \approx 5$–15 h).

iv) Composition fluctuations can be inferred by comparing the shape of H- and δ-distributions for ^{57}Fe and ^{119}Sn, respectively. Although Fe and Sn mix and eventually give rise to a single phase bcc solid solution ($x=0.15$), the distribution of atoms in the bcc structure is not homogeneous: each element tend to be surrounded by atoms of the same species.

v) A stationary state is achieved ($x \leq 0.30$) for $t \geq 15$ h.

2. Mechano-synthesis of Al–Ni–Fe and Al–Cu–Fe alloys

Aluminium readily forms quasicrystalline (qc) alloys with one or more transition metals. Particularly, the most perfect (and stable) quasicrystals known were

found in the ternary system Al-Cu-Fe[7]. The traditional way for preparing them has been the fast-quenching from the melt but they have also been obtained by mechanical alloying (MA) of the elemental constituents[8][9]. Attempts to prepare qc-AlFe alloys by MA have failed[10], yielding simply an amorphous alloy.

We started a research program on the production of qc alloys by MA in Al-TM-Fe systems (TM: Ni, Cu, etc)—particularly the influence of the third alloying element (TM) and the milling device power—and on the evolution of short range order during the milling process. We present here results on the ball milling of pure powder mixtures of nominal composition: $Al_{75}Ni_{10}Fe_{15}$ (Sample 1) $Al_{65}Ni_{20}Fe_{15}$ (Sample 2) and $Al_{63}Cu_{25}Fe_{12}$ (Sample 3).

In the first stages of milling considerable welding occurs and the sample becomes inhomogeneous with large bright aggregates dispersed in a dark fine powder. This welding process continues, giving rise to hard adherences in the ball and the vial. The sample heterogeneity avoided XRD studies at this stage. Also, the nominal milling times t must be taken with care as the effective milling time may be considerably lower. At larger milling times, the sample becomes homogeneous and gradually finer and at this stage the ME spectra evolve indicating that Fe reaction with the other components accelerates.

Figure 5 shows the ME spectra of Sample 1 after different times of milling. Up to 250 h they show a predominant magnetic sextet corresponding to metallic iron together with a minor ($\approx 10\%$ of Fe nuclei) paramagnetic component which is indicative of some reacted regions. No significant variation in the magnetic hyperfine field and isomer shift of the magnetic sextet is observed.

After 400 h of milling the ME spectrum is completely different, with no traces of a magnetic sextet. It may be roughly described as a broad quadrupolar doublet (standard deviation $=0.24_{15}$ mm/s) with average quadrupole splitting $\Delta=0.51_3$ mm/s and $\delta=0.221_3$ mm/s. Better fits were obtained by assuming a Δ-distribution and—in order to take account of the small spectrum asymmetry—by allowing for slight variations in δ from site to site. The XRD pattern of this sample shows rather broad reflections at definite angular positions (see Fig. 6).

After 400 h of milling the samples were encapsulated in evacuated quartz tubes ($p\approx 6\times 10^{-6}$ mbar) and annealed as follows: Sample 1: 20 h at 1073 K, Sample 2: 60 h at 693 K plus 24 h at 1123 K and sample 3: 24 h at 1123 K.

After the heat treatment there is a net reduction in the linewidth of the ME doublet and some changes in their average parameters ($\Delta=0.425_1$ mm/s, $\delta=0.247_1$ mm/s and standard deviation $=0.099_4$ mm/s). The corresponding XRD pattern displays well-defined reflections but keeps resemblance from that of the as-milled sample. This pattern may be indexed with the Al_5Co_2 hexagonal structure which has been reported for the intermetallic $Al_{10}NiFe_3$.

The values quoted for the quadrupole interaction are then representative of the quadrupole interaction at Fe sites in this crystalline phase in the as-milled and annealed states. The main difference between their ME spectra resides in the narrowing of the Δ-distribution and the disappearance of the high Δ components. The latter may correspond to defected environments recovered by the annealing. The average δ approaches the values observed for Al-Fe systems with similar composition.

Figure 5 also shows the ME spectra of sample 2 after different times of milling. Their initial evolution is similar to that observed in sample 1 but the disappearance of the magnetic sextet occurs already after 150 h of milling. The resulting quadrupole spectra is highly asymmetric as expected for a Δ-distribution with an associated monotonously varying δ. This spectrum is similar to that reported for a random bcc-Al(Ni, Fe) alloy obtained by melt- or vapour-quenching[11][12] but the resulting δ is slightly higher indicating Al-richer Fe environments.

With further milling (250 h) the spectra remain paramagnetic with some variations in the Δ-distribution which narrows and shifts to lower mean Δ. With the last

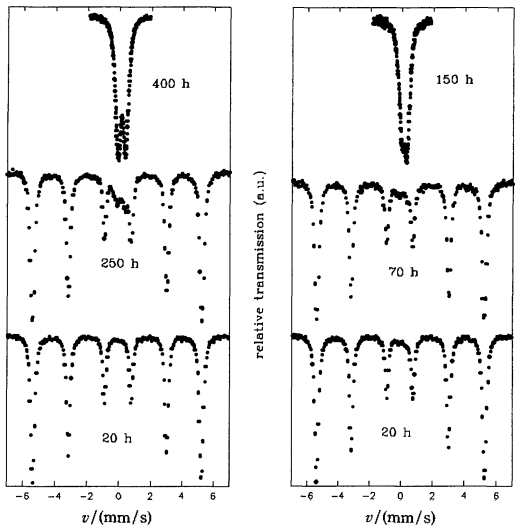

Fig. 5 ^{57}ME spectra of $Al_{75}Ni_{10}Fe_{15}$ (left) and $Al_{65}Ni_{60}Fe_{15}$ (right) after different time of milling.

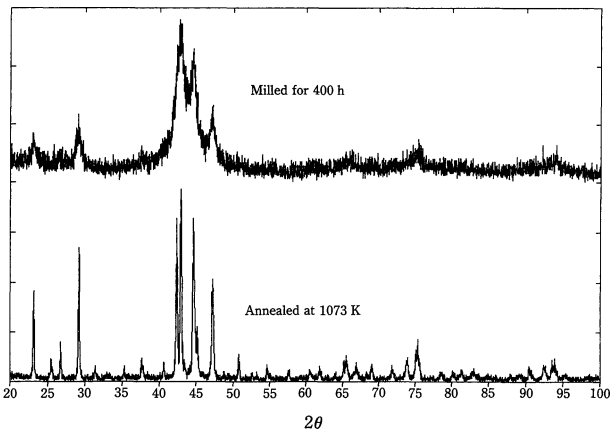

Fig. 6 XRD patterns of $Al_{75}Ni_{10}Fe_{15}$ as milled and annealed at 1073 K.

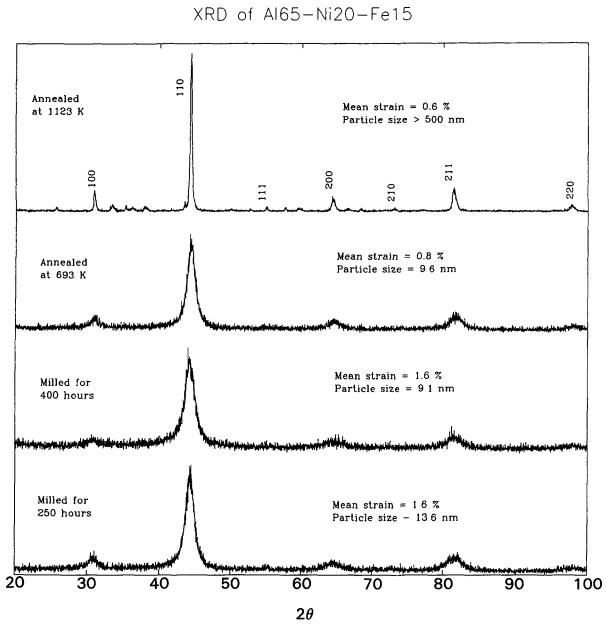

Fig. 7 XRD patterns of $Al_{65}Ni_{20}Fe_{15}$ after different milling times and heat treatments.

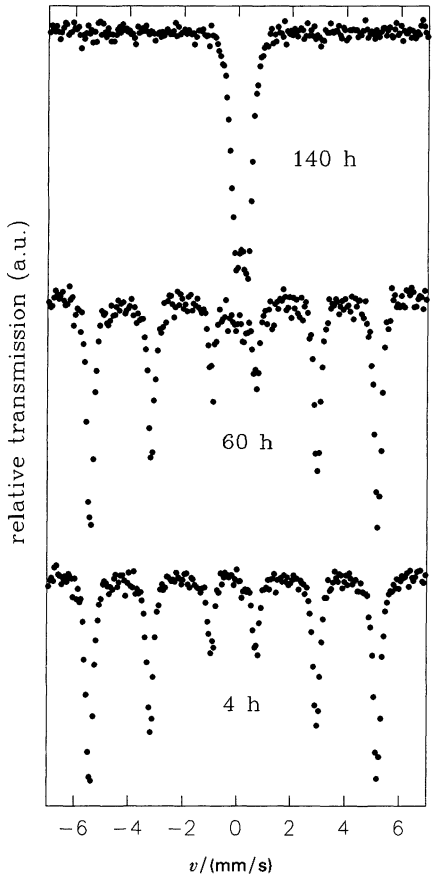

Fig. 8 ^{57}Fe ME spectra of $Al_{63}Cu_{25}Fe_{12}$ after different times of milling.

milling process (400 h) a shoulder (second peak) develops in the Δ-distribution and an overall decrease in δ occurs. This results are corroborated by the XRD patterns (Fig. 7) which may be interpreted as produced by a partially ordered Al(Ni, Fe) alloy with a bcc structure. (Full order would give a B2 structure).

The effect of the heat treatments described above is to reduce considerably the high field contributions to the Δ-distribution. The corresponding XRD patterns show the reflections expected for a partially ordered bcc solid solution that approaches a B2 structure.

All these ME spectra and the resulting Δ-distributions display a non-vanishing probability of having $\Delta=0.0$ associated with 'perfect' Fe environments: first coordination shells occupied by the same kind of atoms (most probably Al). The low and high Δ values in the distribution could be attributed respectively to second- and first-neighbors disorder. This description seems to be confirmed, at least qualitatively, by the presence of well-defined superstructure reflections at 31, 55 and 73° in the XRD pattern of the fully annealed sample.

The XRD patterns show additionally some variations in the reflections linewidth that we interpreted in terms of modifications of the particle size and material strain. They contribute to the linewidth in k-space a constant term and a term linear in k, respectively[13]. From this analysis we obtained the values quoted in Fig. 7. The final milling process further reduces the mean particle size without affecting the existing strain. In turn, this is considerably reduced by the first annealing, while the second one mainly increases the particle size.

The evolution of sample 3 under milling is quite similar (see Fig. 8): the paramagnetic component is already present ($\approx 6\%$ of Fe nuclei) after $t=60$ h and the magnetic sextet disappears after $t\approx 150$ h. The resulting quadrupole spectra after $t\approx 200$ h is centered around $\Delta=0.43_1$ and $\delta=0.24_1$ and the corresponding XRD patterns show the reflections expected for a partially ordered bcc solid solution. The effect of the heat treatment described above is to reduce considerably the high Δ contributions to the Δ-distribution in the ME spectra and to reduce the width of the reflection lines in the XRD pattern. It may be then indexed as a bcc-solid solution with some extra lines that could be assigned to a minoritary icosahedral phase.

In summary, it is clear that, under ball milling, the starting powder mixture goes through two distinct processes. The first one is dominated by the welding of the constituents, mainly due to the great Al content. Actually, in some instances the ball gets stuck to the vial as we have already observed when milling Fe-Sn powder mixtures. Nevertheless some alloying takes place and allows for the gradual material detachment and its submission to further mechanical work. In the second step the main reaction proceeds, under mechanical milling, yielding the final products. Although the employed technique, which probes only the Fe sites, could not yield much information about the first stage it seems evident that while some Fe atoms react with Al and/or Ni/Cu to form the observed paramagnetic phases, bulk Fe itself remains practically pure.

During the second stage the SSR accelerates and after the final milling step there are no traces of a magnetic

interaction in the ME spectra indicating that pure Fe is exhausted and has fully reacted with the other constituents. The observed quadrupole interaction are then characteristic of the resulting, highly defected, final phase or phases. These are: a crystalline intermetallic compound, a partially ordered alloy with bcc structure and a mixture of a bcc alloy with traces of an icosahedral phase respectively for $Al_{75}Ni_{10}Fe_{15}$, $Al_{65}Ni_{20}Fe_{15}$ and $Al_{63}Cu_{25}Fe_{12}$. The heat treatments simply increase the crystallite size and remove the remaining disorder but do not produce structural modifications evidencing the stability (up to about 1100 K) of the phases obtained.

We failed then in obtaining qc-phases by MA and this was probably due to the low specific power supplied by our milling device. More experiments with an enhanced power transfer ability of the milling device are needed in order to investigate the compositional-/specific power-dependence of the qc-formation range.

3. Mechanical grinding of Fe_2B

Mechanical treatment of Fe–B systems have lead to controversial results. Different studies of MA of Fe–B mixtures have apparently yielded different results[14]-[17], suggesting that experimental conditions are very important for this particular system. Recent results on MG of the compound FeB seem to confirm this statement: experiments performed in air induced the decomposition $FeB \rightarrow FeB + Fe_2B \rightarrow FeB + Fe_2B + \alpha\text{-Fe}$, while those carried out in argon or vaccum produced the phase transformation $\beta\text{-FeB} \rightarrow \alpha\text{-FeB}$[18][19]. It must be pointed out, however, that both groups used a higher energy device and longer milling times for grinding in air than for grinding in argon or vaccum. In this section we discuss results of the MG of Fe_2B under argon and air atmospheres.

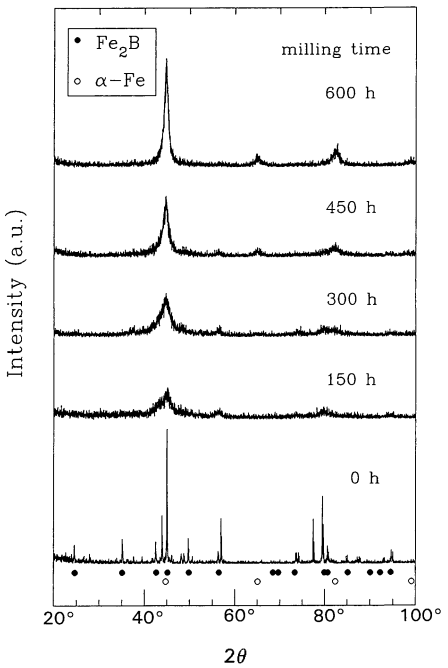

Fig. 9 XRD patterns taken after grinding Fe_2B during different times.

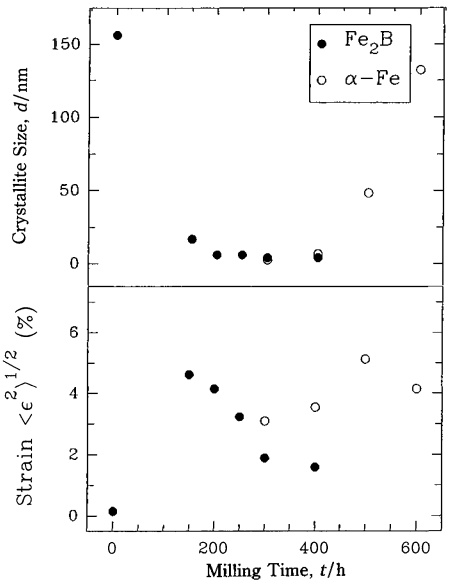

Fig. 10 Mean grain size and rms strain obtained from the XRD patterns taken after different grinding times.

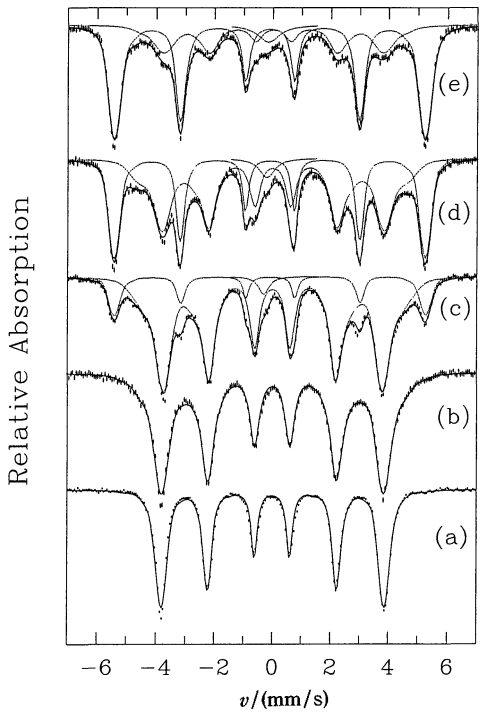

Fig. 11 ^{57}Fe ME spectra taken after grinding Fe_2B during different times.

This work is part of a project devoted to the investigation of MG and MA on Fe–TM–B phases.

Fe_2B powder was encapsulated under high purity argon at atmospheric pressure inside a globe-bag. Five whashings with argon, each followed by moderate vaccum, were performed before encapsulating. The argon supply was constant, being the end of the supplying hose continuously kept at the apertures of the vial parts. (this same procedure was followed with all the systems studied in this work).

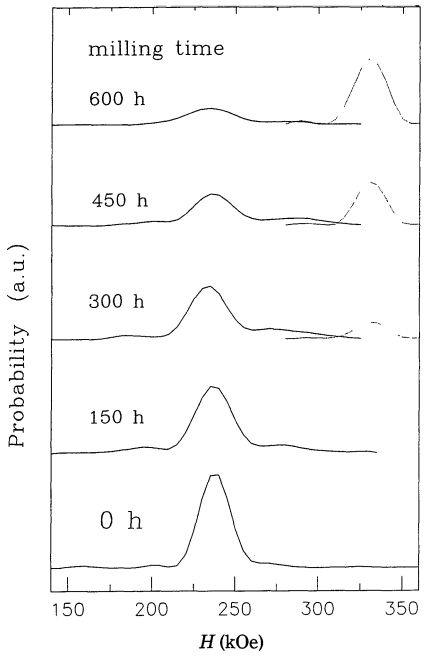

Fig. 12 H-distributions corresponding to ME spectra shown in Fig. 11.

Figures 9–12 show some of the XRD and ^{57}Fe ME results for one grinding run where the ball to powder mass ratio was about three. In Fig. 10, the Fe_2B mean grain size and rms strain obtained from the diffractograms, are displayed. For $t \leq 150$ h, both XRD and ME results indicate that crystallites become smaller and strain increases, but no decomposition is detected. After longer milling times, a reduction of both grain size and strain is observed while formation of α-Fe proceeds at an almost steady rate.

In order to investigate if oxygen contamination during the long grinding runs was responsible for Fe_2B decomposition (as was proposed for the decomposition of FeB by MG[19]), two other experiments where performed. In one of them the vial and Fe_2B powder were kept inside a latex baloon which was connected to a vaccum diffusion system and to the high purity argon supply. A higher than atmospheric pressure was always kept inside the argon branch in order to minimize the risk of air intake. Four washings with argon were carried out, each followed by pumping down to 10^{-2} mbar. Next, pressure was reduced to about 10^{-5} mbar and maintained for about two hours. Afterwards, three more argon washings were performed. Finally, the vial was closed in argon at one atmosphere and sealed with a wide latex ribbon without opening the baloon, and then the baloon itself was sealed at three different positions (so that a fourfold barrier for air contamination was built). In addition, ball to powder mass ratio was increased to 20 in order to reduce grinding processing time. The ME and XRD results obtained for $t=94$ h are shown in Fig. 13. They clearly indicate that about 40% of the Fe is in the form of α-Fe. For oxygen to be effective in retaining boron atoms at grain surfaces, a minimum number N_O of O atoms would be needed for a given number N_B of B atoms. Assuming that at least one of the near neighbours to a boron atom must be oxygen, we will need $N_O \approx 0.1\ N_B$. For a vial of 5 cm^3 filled with air at atmospheric pressure and containing 0.150 g of Fe_2B, $N_O \approx 5.6 \times 10^{19}$, $N_B \approx 7.3 \times 10^{20}$, and $N_O/N_B \approx 0.08$. Oxygen contamination in quantities comparable to this is very unlikely in the experimental conditions described above and can therefore be discarded as the fundamental cause of the observed decomposition.

The second experiment was performed after sealing the vial under normal air atmosphere, but otherwise in the same experimental conditions as before. Although the reaction products were not identified yet, the results shown in Fig. 13 indicate that massive oxygen contamination has very dramatic and distinctive effects, which clearly affect iron environments as well. Experiments are in progress to determine if oxygen, nitrogen, or both are resposible for these results.

It is then proposed that the decomposition $Fe_2B \rightarrow \alpha\text{-Fe} + B$ occurs by MG. Since boron has been identified as the mobile species in Fe_2B[20], it is suggested that part of the mechanically transferred momentum produces boron diffusion. As the grain size decreases the probability

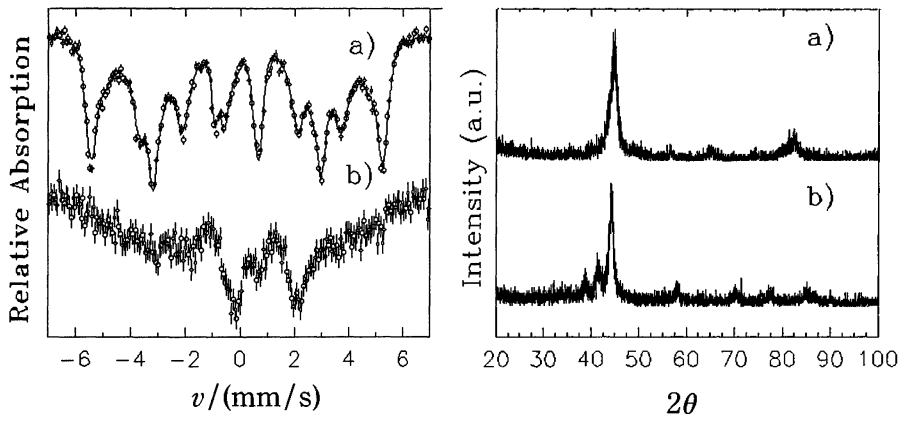

Fig. 13 ^{57}Fe ME spectra and XRD patterns corresponding to vial sealed in argon after high vaccum treatment (top) and vial sealed in normal air atmosphere (bottom).

for a B atom to reach a crystallite border increases. We have estimated that for crystal sizes of the order of those in Fig. 10 (200 h, 4 nm), the separation of Fe_2B in α-Fe+B may become energetically favorable[21]. The identification of oxygen as the main responsible for Fe_2B decomposition is not supported by the present experiments. More experiments varying the power transfer ability of the milling device as well as the gas environment, in a systematic manner, are needed in order to fully elucidate this question.

IV. Summary and Conclusions

Mössbauer effect spectroscopy has been applied to the study of mechanical alloying of Fe–Sn, Al–Ni–Fe, and Al–Cu–Fe, and mechanical grinding of Fe–B. By this means the atomic configurations at sites occupied by especific constituents have been probed. Combined with X-ray diffraction analysis this experimental approach has allowed the observation of the following features:

(1) Formation of $FeSn_2$ in superparamagnetic state for crystal sizes of at most 70 nm.

(2) The existence of important composition fluctuactions in metastable bcc Fe–Sn solid solution.

(3) Formation of stable (disordered) crystalline phases in the Al–Ni–Fe and Al–Cu–Fe systems and its hyperfine characterization.

(4) Ordering induced by ball milling in the bcc structure of the $Al_{65}Ni_{20}Fe_{15}$ alloy.

(5) Absence of boron or eventual contaminants in the α-Fe segregated from Fe_2B submitted to MG under argon atmosphere.

Acknowledgement

The authors wish to acknowledge the finantial support from Consejo Nacional de Investigaciones Científicas y Tecnológicas (CONICET) of the Republica Argentina.

REFERENCES

(1) G. Le Caër, P. Matteazzi and B. Fultz: J. Mater. Res., **7** (1992), 1387.
(2) S. Nasu, P. H. Shingu, K. N. Ishihara and F. E. Fujita: Hyp. Int., **55** (1990), 1043.
(3) F. R. de Boer, R. Boom, W. C. M. Mattens, A. R. Miedema and A. K. Niessen: *Cohesion in Metals, Transition Metal Alloys*, Vol. 1, Ed. by F. R. de Boer and D. G. Pettifor, North-Holland, Amsterdam, (1988), p. 244.
(4) A. F. Cabrera, F. H. Sánchez and L. A. Mendoza Zélis: unpublished.
(5) I. Vincze and A. Aldred: Phys. Rev., **B9** (1974), 3845.
(6) R. Ingalls, F. Van der Woude and G. A. Sawatzky: *Mössbauer Isomer Shifts*, Ed. by G. K. Shenoy and F. E. Wagner, North-Holland, Amsterdam, (1978), p. 409.
(7) A. P. Tsai, A. Inoue and T. Masumoto: Jpn. J. Appl. Phys., **26** (1987), L1505.
(8) J. Eckert, L. Schultz and K. Urban: Appl. Phys. Lett., **55** (1989), 117.
(9) J. Eckert: *Mechanical Alloying, Proceedings of the International Symposium on Mechanical Alloying*, Kyoto, 1991, Trans Tech Publications, Zürich, (1992), p. 679.
(10) G. Wang, D. Zhang, H. Chen, B. Lin, W. Wang and Y. Dong: Phys. Lett., **A155** (1991), 57.
(11) A. P. Tsai, N. Kataoka, A. Inoue and T. Masumoto: Jpn. J. Appl. Phys., **29** (1990), L1696.
(12) A. P. Tsai, N. Kataoka, A. Inoue and T. Masumoto: Sci. Rep. RITU, **A-36** (1992), 300.
(13) M. Atzmon, K. M. Unruh and W. L. Johnson: J. Appl. Phys., **58** (1985), 3865.
(14) A. N. Campbell, J. C. Barbor and C. R. Hills: J. Mater. Res., **4** (1989), 1303.
(15) J. Jing, A. Calka and S. J. Campbell: J. Phys.: Condens. Matter, **3** (1991), 7413.
(16) S. Suriñach, M. D. Baró, J. Segura and N. Clavaguera-Mora: Mater. Science Forum, **88–90** (1992), 275.
(17) H. Shirahata and M. Nagumo: Report of Materials Science and Technology, Waseda University, **42** (1991), 15.
(18) A. Ye. Yermakov: *Mechanical Alloying, Proceedings of the International Symposium on Mechanical Alloying*, Kyoto, 1991, Trans Tech Publications, Zürich, (1992), p. 577.
(19) J. Balogh, L. Bujdosó, Gy. Faigel, L. Gránásky, T. Kemény, I. Vincze, S. Szabó and H. Bakker: Nanostructured Mater., **11–18** (1993), 11.
(20) C. M. Brackman, A. W. J. Gommers and E. J. Mittemeijer: J. Mater. Res., **4** (1989), 1354.
(21) C. Rodríguez Torres, F. H. Sánchez and L. Mendoza-Zélis: unpublished.